Sensing and Imaging (2019) 20:28
https://doi.org/10.1007/s11220-019-0251-1

ORIGINAL PAPER

# Analysis of Performance of Howland AC Current Source for Electrical Impedance Spectro-Tomography

**Reza Ghorbani**[1] · **Manoochehr Nahvi**[1]

Received: 9 January 2019 / Revised: 15 June 2019 / Published online: 24 June 2019


## Abstract

Electrical impedance tomography (EIT) is a technique that is able to deliver valuable information on conductivity distribution in a process. An extension to conventional EIT is electrical impedance spectro-tomography (EIST) which is offering spectroscopic information. Along with methodological advancement of EIST and to meet practical requirements, there are ongoing researches to develop proper high-quality EIST hardware. An important part of EIST hardware is voltage controlled current source which its design is appeared to be a challenging task. This paper addresses briefly the aspects of EIST system and discusses the effect of various factors and their joint impacts on commonly used Howland voltage controlled current sources for EIST application. To perform realistic simulations, practical load and electrode model are applied within sensing bandwidth. The simulation results revealed the considerable impact of resistors tolerance on reducing the output impedance of the current sources in low frequencies while increasing the operating frequency significantly reduces the impact of tolerance. The simulation also demonstrates that the load current relative error is directly proportional to the resistors' tolerance and its value approaches the ideal state, with zero-tolerance resistors, by increasing operating frequency. This point can be employed to determine the minimum operating frequency in which the impact of resistors tolerance can be canceled. The results imply that by using resistors with a lower tolerance, it is possible to achieve wider bandwidth in EIST. It can also be concluded that dual op-amp Howland current source is a suitable choice for EIST application.

**Keywords** Electrical impedance tomography · Electrical impedance spectro-tomography · Impedance spectroscopy · EIST hardware · Voltage controlled current source · Howland current source

✉ Manoochehr Nahvi
nahvi@guilan.ac.ir

[1] Department of Electrical Engineering, Faculty of Engineering, University of Guilan, Guilan, Iran

## 1 Introduction

Electrical Impedance Tomography (EIT) is an electrical tomographic method that is able to deliver valuable information and images from a process by non-destructive measurements. This method was first introduced in 1978, and it is applied for estimating the electric conductivity distribution within a process [1]. Given its relative simplicity of implementation, high speed, and low cost, this method successfully has been entered into industrial and medical applications [2]. In this technique, by injecting a stable AC current and measuring the amplitude and phase of voltage values on the electrodes placed at the boundary of the process, it is then possible to reconstruct an estimation of the electrical conductivity distribution and capacitive property of the process using modeling and numerical methods [3]. This method can be conducted in two modes; single-frequency EIT or multi-frequency EIT (MFEIT). In multi-frequency mode, if the process contains materials with frequency dependent characteristics, the resulted measurements are also different at any given frequency. Thus, the reconstructed images are also different at different frequencies. By perusing these images at different frequencies, one can likely obtain valuable spectral information of a process and its inside materials [4]. Since in MFEIT the input sinusoidal current source generally contains two or several frequency components, a proper design for the required hardware including current source, voltage measurement circuitries, and data acquisition system is necessary [5]. In Ref. [6], a new generation of MFEIT was provided for extending conventional MFEIT to a spectral EIT system so-called electrical impedance spectro-tomography system (EIST) using wideband chirp as excitation current. The essential principle of EIST is frequency-dependent behavior of process materials in responding to an input spectral excitation current [4].

This system employs a one-shot chirp excitation signal which provides simultaneous fast spectral measurements in a much faster manner. In this method, there is no need to perform a single frequency acquisition at several different frequencies. Using these spectral measurements, tomographic images at desired frequencies can be reconstructed. In [2, 4], the feasibility of the spectro-tomography method is examined using a fast single-channel system and performing several experimental trials in a crystallization process. In [7], the experimental arrangement of such method is further discussed and justified by comparison the results with those obtained with a commercial spectrum analyzer.

In impedance spectroscopy and EIST systems, an accurate and stable current source is necessary over sensing bandwidth. To improve the performance of current sources, several attempts have been reported in the literature. Due to reasons that would be discussed in Sect. 3, designing AC current sources is an existing challenge in the discrete implementation and integrated circuits layout-designs [8]. In this regard, the main aim of the present study is analyzing the impacts of various factors affecting the designing of an AC current source for EIST applications.

In what follows an overview of EIST system is given in Sect. 2. Then, the requirements of current sources for EIT systems and various Howland structures

for using as a current source will be discussed in Sect. 3. The factors affecting the performance of different structures of the aforementioned current sources are evaluated in Sect. 4. In Sect. 5, Howland current sources are analyzed and discussed with the focus on EIST application. Finally, concluding remarks are provided in Sect. 6.

## 2 Overview of Electrical Impedance Spectro-Tomography (EIST)

Electrical impedance tomography is commonly applied at a specific frequency. However, if process materials show frequency-dependent characteristics, prior information about the process and its inside materials are required to achieve a desirable performance of the method. Different responses of these materials to the input excitation frequency will affect the voltage values measured at peripheral electrodes and thus reconstructed images. For instance, impedance spectral characteristics of a pharmaceutical material, called L-glutamic acid, LGA, during a crystallization process [4]. In such processes, therefore, choosing appropriate operating frequency is an important issue in exploiting EIT. The variation of material's behavior in responding to an input excitation signal at different frequencies is the main idea of EIST [6]. Experimental verifications of EIST system for process sensing and imaging are presented in Refs. [2] and [9].

Figure 1 shows the conceptual equivalent circuit of EIST system based on adjacent sensing method. In the adjacent sensing method [10], the current is injected between a pair of adjacent electrodes and corresponding voltage measurements are conducted through the remaining electrodes at every step of measurement. The

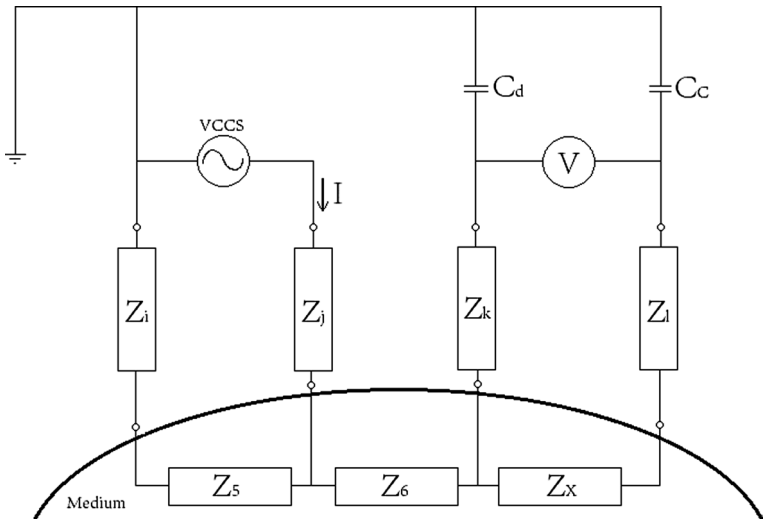


**Fig. 1** Conceptual equivalent circuit of EIST system based on adjacent sensing method

process is continued in a sequential manner until every adjacent pair of electrodes are utilized for current injection.

In Fig. 1, $z_i, z_j, z_k$, and $z_l$ are the peripheral electrodes' impendence values and $C_c$ and $C_d$ are coupling capacitors. $z_5$, $z_6$, and $z_x$ indicate the impedances of a process. In general, the values of these impedances may vary owing to the frequency-dependent characteristics of the process and also the measurement method. In every step of adjacent sensing method, electrodes' impendence values and $z_5$ can be almost assumed constant.

However, $z_6$ and $z_x$ values vary at every step with the changing of voltage measurement electrodes position and impedance characteristic of the process [7]. In general, in an EIST system, the relation between spectral excitation current $i_e(t)$ and its response on the peripheral measuring electrodes, $v_m(t)$, may be expressed as:

$$Z(x, y, z, t, f) = \frac{|V_m(f)|}{|I_e(f)|} e^{j(\angle V_m(f) - \angle I_e(f))} \tag{1}$$

where $x, y, z$ are the positions of the measured impedance, $t$ is the time, and $f$ is the frequency at which the measurement applied. $I_e$ and $V_m$ are estimated from input spectral excitation current and corresponding spectral measurement voltage.

Two important stages in developing an EIST system are the selection and synthesis of an appropriate wideband excitation signal and designing a wideband AC current source. Given this, for analyzing a process behavior or materials, it is vital to estimate the sensing bandwidth for the appropriate synthesis of the excitation signal. For this, prior knowledge regarding the material inside a specific process may be very useful. If one is able to determine the minimum ($\tau_{min}$) and maximum ($\tau_{max}$) first-order time constant values based on the materials existing in the process, it may be possible to approximately determine the appropriate bandwidth $\Delta\omega$ of the input signal based on the following equation:

$$\frac{1}{\alpha \tau_{max}} \leq \Delta\omega \leq \frac{\beta}{\tau_{min}} \tag{2}$$

where α and β are arbitrary factors for appropriate adaption of the bandwidth [4, 11].

For realizing the frequency analysis of a process using EIST system, it is required to select one of the wideband signals such as multi-frequency compound sinusoidal, pseudo-random binary, pulse, Sinc, and Chirp signals as the input of the voltage-controlled current source (VCCS). In Refs. [12, 13], a comprehensive comparison has been provided regarding the characteristics of these signals and concluded that Chirp signals could be an appropriate choice for simultaneous spectral excitation. Through using Chirp, it is possible to optimize both sensing bandwidth and duration. Figure 2 indicates an example of reconstructed images of a process at different frequencies using a linear Chirp. Although using existing hardware, generation of Chirp is easy, it is required to employ a relatively complicated algorithm, as presented in Ref. [14], for extraction of the necessary information from the spectral measurements for the purpose of reconstruction of tomographic images at desired frequencies.

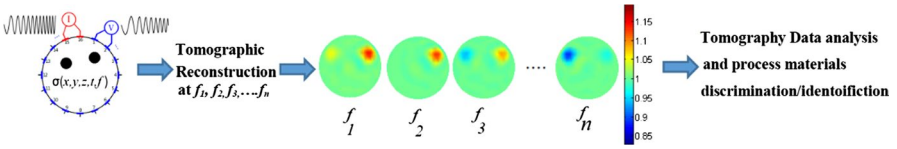


**Fig. 2** Conceptual Procedure of an EIST system, (the Chirp and tomographic images are synthetic)

Moreover, the non-linear and frequency-dependent behavior of the process may cause the inappropriate performance of the current source over sensing bandwidth. In practice, thus, in designing an EIST system, it is necessary to design an AC current source which would be able to provide a stable behavior throughout the operating frequency range. Further, as stated earlier, in this range the magnitude and phase of the output current required to remain constant to an acceptable level, so that conducting appropriate spectral measuring is possible for the purpose of tomographic reconstruction [15]. In Ref. [16] the impact of resistor mismatches and Op-amp GBW on the output impedance of the Howland current source are discussed for conventional EIT systems. The designing of such a current source is considered as one of the important challenges of the EIST systems. The motivation of the present study is thus analyzing the factors affecting the designing of the current source and their joint impacts.

## 3 Overview to Current Sources for Electrical Impedance Tomography Systems

In EIT and EIST systems, an essential requirement is to have high accuracy and stable current source. To achieve this, theoretically, an ideal current source would have infinite output impedance and no dependency on operating frequency and also load characteristics. This is however practically not achievable. This is due to the numerous reasons and limitations including non-ideal and frequency-dependent characteristic of circuit devices, stray capacitances, wide sensing bandwidth, load dynamic range and its frequency dependence, resistors' tolerance and their mismatch [14–18].

To design the current source in an EIST system for medical and industrial application, a further critical need is the stability and accuracy of the current source over the desired frequency range. Therefore, usually, the current sources are designed such that they meet the requirement needed for a specific application. For instance, the typical parameters' values for industrial and medical applications are distinctly different. The parameters in the industrial application are mostly dependent to process material and the rig dimension while in the medical application, there are further safety issues [14, 19].

In literature, two main types of current sources for EIT systems, consisting of the voltage-controlled current source (VCCS) and current sense voltage sources (CSVS), have been presented [20]. Among the two above categories, the VCCS is very common in EIT systems. In VCCS, ideally, the output current must linearly follow the input voltage and remains stable over load and frequency range. Figure 3 demonstrates some examples of VCCS circuits.

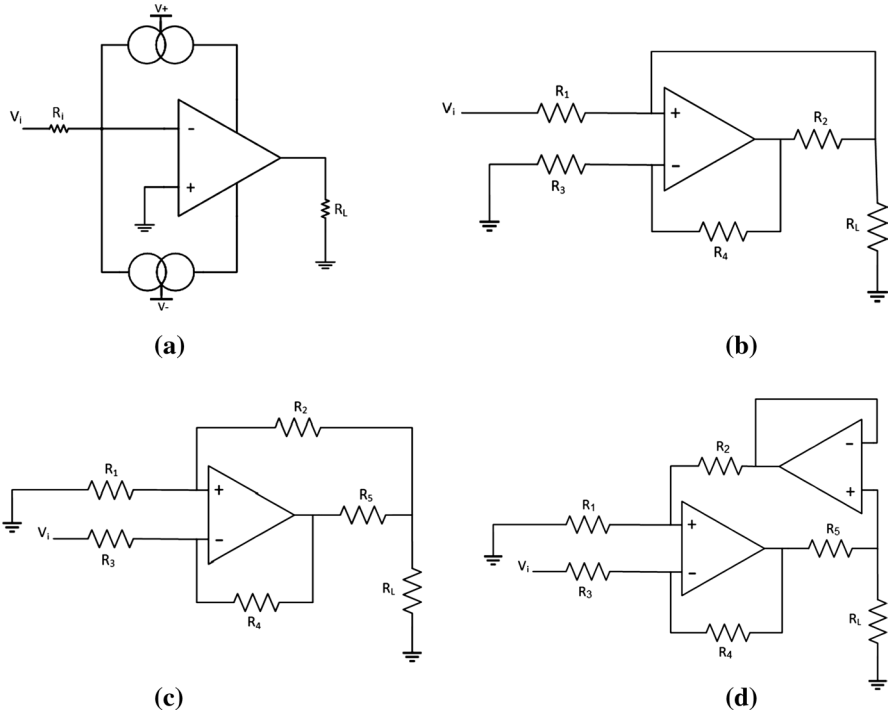


**Fig. 3** Examples of VCCS circuits

Figure 3a shows a supply-current sensing current source [21, 22]. In this type, the variation in the load current is mirrored to the op-amp inverting input, and thus the load current is adjusted. The output impedance of this type was reported about 290 KΩ at the frequency of 160 kHz. Another high precision VCCS compensated by a network parallel to the load and controlled by a computer is presented in [23]. Despite the high output impedance of this type, which was more than 50 MΩ at the frequency of 30 kHz, it suffers from limited bandwidth.

The Howland current source in which the voltage feedback was used, as shown in Fig. 3b, employed as the current source for EIT application in [24]. In [25], a high bandwidth modified Howland current source is presented for medical application, as in Fig. 3c. The output impedance of the current source is improved using a generalized impedance converter (GIC) in parallel with the output load. This results in a simulated output impedance better than 2 G over the frequency range of 100 Hz to 1 MHz, while the biggest experimental impedance was 143 M at 1 kHz. However, the long procedure of current adjustment makes it difficult to use this type of current sources for MFEIT or EIST system. The modified Howland current source was also employed in the Sheffield MK3.5 system [26]. This current source gives a peak-to-peak 850μA and results in maximum output impedance of 750 kΩ at 10 kHz. A dual op-amp current source for industrial application is reported in [27], as shown in Fig. 3d. It delivers 30 mA current over discrete frequency point in the range of 75 Hz to 153.6 kHz, and maximum output impedance of 2.5 MΩ at 76.8 kHz is reported. Operational transconductance

amplifiers (OTA) are reported in the literature as VCCS, for instance in [28, 29]. They have the advantages of less required peripheral circuitry, stability over frequency and load ranges, and also wide bandwidth. Their disadvantages are the limitation of the output impedance and maximum output current. In [28], a current source using CCII01 is reported for UCLH Mark 1b, operating over frequency 225 Hz to a maximum of 77 kHz with an output impedance of 537 kΩ parallel to 28 pF. The operational amplifier AD844 [29] has been employed to build the current source, for instance, in [30–32]. The special internal structure of this wideband amplifier, which is the high impedance slewing pin (TZ), gives the capability of using AD844 as a VCCS. In [30], AD844 is used for designing a current source in the frequency range of 10–250 kHz. Its output impedance was better than 1 MΩ in parallel with 5pF capacitance [32]. In [31], a high output current source using a parallel structure of eight AD844 s is reported, and its output impedance was about 750 kΩ in parallel with 18pF.

The most common structures which have been used in EIT systems are Howland current sources which are also known as voltage feedback current sources. In this type of current sources, there are some other complementary circuits added to the main circuit such as the generalized impedance converter (GIC) to improve its output impedance [25, 33, 34]. The Howland current sources, according to the load position, are categorized into two main classes, consist of floating load and grounded load. In most cases, grounded-load current source is employed [35]. Therefore, in continue, different structures of Howland current source with grounded-load are comparatively presented.

### 3.1 Basic Howland Current Source

Howland current source was originally invented by Professor Bradford Howland, and its structure was first published in 1964 [24, 33]. According to Fig. 3b, this current source has both positive and negative feedbacks, and it is thus likely to oscillate at high frequencies [36]. To avoid oscillation, two 10 pF capacitors were connected in parallel with feedback resistors. At low-frequency applications, there is however no need to this compensation. The main drawback of the basic Howland current source is its power consumption. To overcome this problem, its improved structure is provided in Ref. [36] in which the $R_2$ resistor is divided into two resistors.

### 3.2 Improved Howland Current Source

The improved Howland current source structure is shown in Fig. 3c. Assuming the ideality of the operational amplifier, it can be proofed that the output current of improved Howland current source is:

$$I_L = -V_i\left(\frac{R_1R_4 + R_2R_4}{R_3R_5\left(R_1 + R_2\right)}\right) + V_L\left(\frac{R_1R_4 - R_3\left(R_2 + R_5\right)}{R_3R_5\left(R_1 + R_2\right)}\right) \tag{3}$$

where $V_i$ is the input voltage,$V_L$ is the the load voltage and $I_L$ is the the output current.

According to the Eq. 3 and for the correct operation of the circuit as a VCCS in Fig. 3c, by zeroing the coefficient of load voltage, the current source would be independent of the load. This is expressed by:

$$R_1R_4 - R_3\left(R_2 + R_5\right) = 0 \Rightarrow \frac{R_1}{R_2 + R_5} = \frac{R_3}{R_4} \tag{4}$$

In general, by taking into account the non-ideality of the operational amplifier, the output current of improved Howland current source is calculated by the following equation:

$$\begin{aligned} I_L = &-V_i\left(\frac{aR_4\left(R_1 + R_2\right)}{R_5\left(R_1 + R_2\right)\left(R_3(1 + a) + R_4\right)}\right) \\ &+ V_L\left(\frac{aR_1\left(R_3 + R_4\right) - R_5\left(R_3(1 + a) + R_4\right) - \left(R_1 + R_2\right)(R_3(1 + a) + R_4)}{R_5\left(R_1 + R_2\right)\left(R_3(1 + a) + R_4\right)}\right) \end{aligned} \tag{5}$$

where $a$ is the gain of the non-ideal operational amplifier.

### 3.3 Dual Op-Amp Howland Current Source

For increasing the output impedance of improved Howland current source, an operational amplifier is added as a voltage follower in one of the feedback paths of the improved Howland current source circuit [33]. The circuit in Fig. 3d is obtained by adding a voltage follower to the positive feedback path of the improved Howland current source. Assuming the ideality of both operational amplifiers, it can simply be proofed that the output current of dual op-amp Howland current source is:

$$I_L = -V_i\left(\frac{R_1R_4 + R_2R_4}{R_3R_5\left(R_1 + R_2\right)}\right) + V_L\left(\frac{R_1R_4 - R_2R_3}{R_3R_5\left(R_1 + R_2\right)}\right) \tag{6}$$

In this equation for eliminating the dependence of the output current to the load, it is required that the values of resistors satisfy the following equation:

$$R_1R_4 - R_2R_3 = 0 \Rightarrow \frac{R_1}{R_2} = \frac{R_3}{R_4} \tag{7}$$

In general, by considering the non-ideality of operational amplifiers, the output current is determined by the following equation:

$$\begin{aligned} I_L = &-V_i\left(\frac{a_1\left(1 + a_2\right)R_4\left(R_1 + R_2\right)}{\left(1 + a_2\right)R_5\left(R_1 + R_2\right)\left(R_3\left(1 + a_1\right) + R_4\right)}\right) \\ &+ V_L\left(\frac{a_1a_2R_1\left(R_3 + R_4\right) - \left(1 + a_2\right)\left(R_1 + R_2\right)\left(R_3\left(1 + a_1\right) + R_4\right)}{\left(1 + a_2\right)R_5\left(R_1 + R_2\right)\left(R_3\left(1 + a_1\right) + R_4\right)}\right) \end{aligned} \tag{8}$$

where $a_1$ is the gain of direct path operational amplifier and $a_2$ is the gain of the operational amplifier in the feedback path.

## 4 Impacts of Various Factors in Performance of Howland Current Source

As mentioned in the introduction, due to the several reasons such as the tolerance of resistors and their mismatch, non-ideal characteristics of operational amplifiers, frequency-dependent behavior of circuit components and sensing bandwidth, the frequency response of current sources may deviate from the desired response. This section presents the impacts of operating frequency and also resistances' tolerance and their joint impacts on the performance of improved Howland current resources and dual op-amp Howland current source. For the proper functioning of these structures, the Eqs. 4 and 7 need to be satisfied. However, due to the existence of tolerance in the circuit resistors, it seems impossible to meet the conditions stated in Eqs. 4 and 7. This can, in turn, reduce the output impedance of the current source and thus affect the amplitude of the output current.

The output impedance, $Z_o = \frac{\partial V_L}{\partial I_L}$, of improved and dual op-amp Howland current sources with non-ideal operational amplifiers can be calculated by Eqs. 9 and 10, respectively, as below:

$$Z_o = \frac{R_5\left(R_1 + R_2\right)\left(R_3(1+a) + R_4\right)}{aR_1\left(R_3 + R_4\right) - R_5\left(R_3(1+a) + R_4\right) - \left(R_1 + R_2\right)(R_3(1+a) + R_4)} \tag{9}$$

$$Z_o = \frac{\left(1 + a_2\right)R_5\left(R_1 + R_2\right)\left(R_3\left(1 + a_1\right) + R_4\right)}{a_1 a_2 R_1\left(R_3 + R_4\right) - \left(1 + a_2\right)\left(R_1 + R_2\right)\left(R_3\left(1 + a_1\right) + R_4\right)} \tag{10}$$

In order to conduct frequency analyzes of the current resources, the operational amplifier is considered to be a single pole system. Thus, the gain, $a$, of non-ideal operational amplifiers in the above equations is:

$$a = \frac{a_0}{1 + j\frac{\omega}{\omega_b}} \tag{11}$$

where $a_0$ and $\omega_b$ are DC open loop gain and bandwidth of the amplifier, respectively [37]. Using Eq. 11, it can be inferred the output impedance of current sources is a function of the operating frequency. For simulation purpose, in this paper $a_0$ and *GBW* are set to $10^4$ and $10^8$ ($\omega_b = 10^4$), respectively.

To study the joint impacts of the resistors' tolerance and operating frequency on the output impedance of currents sources, several simulations were conducted, all simulations performed using MATLAB R2016a. To do so, the output impedance of 10,000 current sources was calculated at each simulation. The input voltage of the VCCS was equal to 1 V p–p and the resistor values for the improved

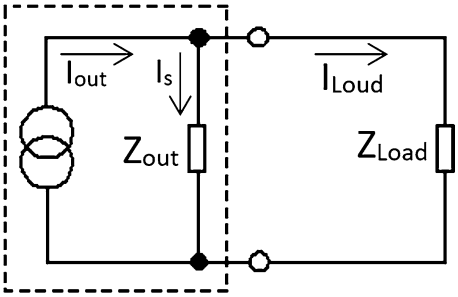


**Fig. 4** Practical current source driving an impedance

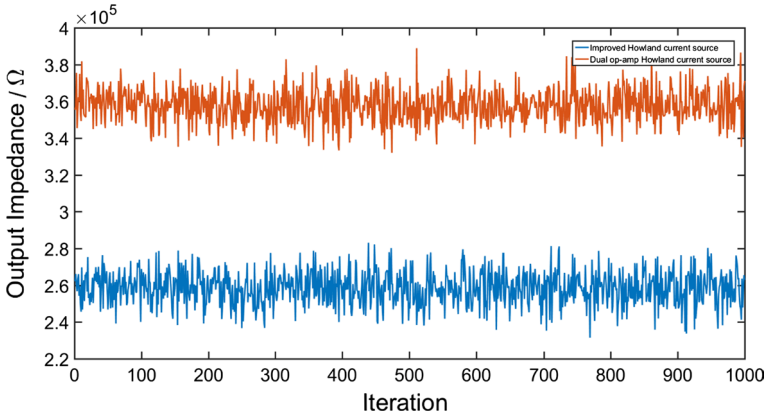


**Fig. 5** Minimum output impedance for Howland current sources in 1000 simulation

Howland current source were $R_1 = R_2 = R_3 = R_5 = 1\,\text{k}\Omega$,$R_4 = 2\,\text{k}\Omega$; in the case of dual op-amp Howland current source, these values were $R_1 = R_3 = R_5 = 1\,\text{k}\Omega$, $R_2 = R_4 = 2\,\text{k}\Omega$. These values were considered in order to provide equal feedback coefficient and current amplitude. By substituting these values in Eqs. 5 and 8, the output current amplitude would be 2 mA p–p.

The minimum acceptable value for output impedance, $Z_{out}$, is calculated by using the Eq. 12 inferred from Fig. 4.

$$I_{Loud} = I_{out} - I_s = \frac{Z_{out}}{Z_{out} + Z_{Load}} I_{out} \tag{12}$$

In this equation, $I_{out}$ is the output current, $I_s = Ec(\%) \times I_{out}$, $E_c$ is the assumed error for the output current amplitude and $Z_{Load}$ represents the load impedance. Figure 5 exhibits the values of the minimum output impedance of the current sources for 1000 times simulation at the operating frequency of 1 kHz and the tolerance of the resistors set to 0.1%. Despite the high gain value at this frequency ($a \cong 9.95 \times 10^3$, according to Eq. 11), the output impedance of the current sources drops down, in average, to 258 k$\Omega$ for the improved Howland current source and 359 k$\Omega$ for the dual

op-amp Howland current source. These values clearly indicate the impacts of tolerance of the circuit resistors in the output impedances.

In order to evaluate the joint impact of the tolerance and operating frequency on the output impedance, the output impedance is calculated over a tolerance range from 0.1 to 1% and the frequency range from 1 kHz to 1 MHz, the results shown in Fig. 6. As can be observed, the output impedance decreases with increasing operating frequency over the range of tolerance. However, the variation of the tolerance of resistors in low frequencies has a significant impact on the output impedance; whereas, with an increase in the frequency, the tolerance effect on output impedance is significantly diminished.

Figure 7 shows the variation of the output impedance at selected frequencies for different tolerances. The figure reveals the insignificant impact of tolerance at high frequencies. It also shows that dual op-amp Howland current source provides higher output impedance in comparison with improved Howland current source.

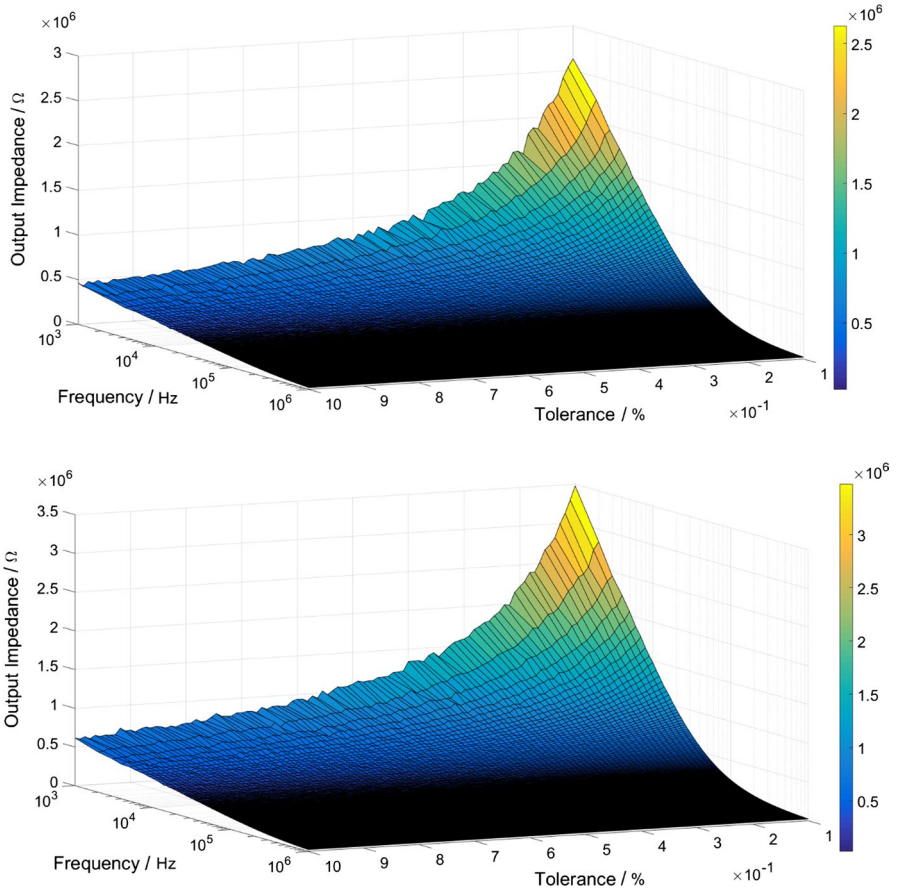


**Fig. 6** Joint impacts of resistors tolerance and operating frequency on output impedance, Improved Howland current source (top) and dual op-amp Howland current (bottom)

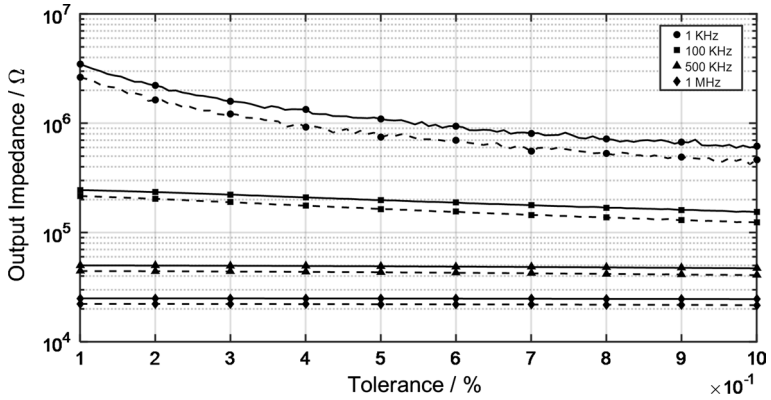


**Fig. 7** Joint impacts of resistors tolerance and operating frequency on output impedance, improved Howland current source (dashed) and dual op-amp Howland current (solid)

## 5 Analyzing Howland Current Source for EIST Application

Since the nature of a frequency-dependent process is not purely resistive and has capacitive behavior, it causes frequency-dependent loading impact on EIST systems. For the impedances mentioned in EIST equivalent circuit model given in Fig. 1, there are two commonly used practical load models [38], as shown in Fig. 8. For these models, different values have been reported for medical and industrial applications, for instance in Refs. [39] and [40]. In this paper, in order to perform feasible simulations, the model parameters are set according to the mature human thorax with values of $R_{1B} = 19.9\Omega$, $R_{2B} = 19.86\Omega$ and $C_B = 99.7pF$ for model B in Fig. 8, as presented in Ref. [39]. In addition, the impacts of peripherally connected electrodes for injecting excitation current and measuring voltages should also be

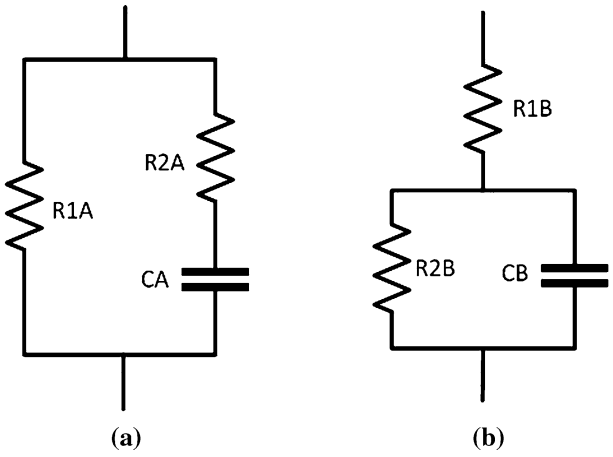


**Fig. 8** Practical load model for electrical impedance tomography

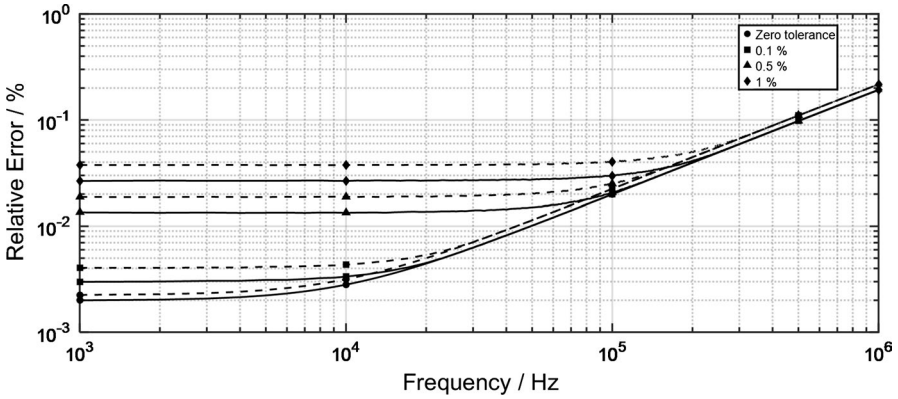


**Fig. 9** The relative error of load current for improved Howland current source (dashed) and dual op-amp Howland current source (solid) with practical load existence in selected resistor tolerances

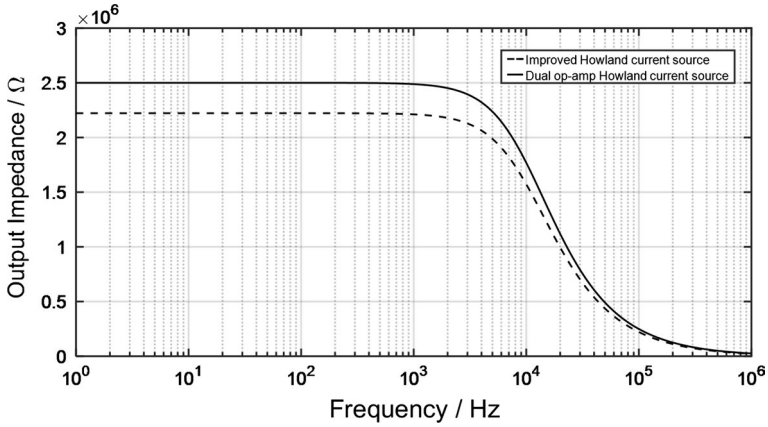


**Fig. 10** Current source output impedance for improved Howland current source (dashed) and dual op-amp Howland current source (solid)

considered for more accurate process modeling. For modeling peripheral electrodes, assuming Silver–Silver Chloride electrodes (Ag–AgCl), a parallel combination of a 240 $\Omega\psi$ resistor and a 240 μF capacitor in series with a 5 $\Omega\psi$ resistor is employed [40].

Based on the models presented in Figs. 1 and 8, improved Howland current source and dual op-amp Howland current source were investigated by taking into account the impact of current injection electrodes and the practical load model. Figure 9 indicates the relative error of the load current amplitude in the presence of practical models and considering the tolerance of circuit resistors. As it can be observed, the relative error has an increasing trend versus frequency. The reason for this can be explained using Eqs. 9 and 10 which are indicating the reduction of current source output impedance versus frequency, as shown in Fig. 10. Based

**Table 1** Tolerance neutralization frequency in improved Howland source and Dual op-amp Howland current source

| Tolerance | 0.1% (kHz) | 0.5% (kHz) | 1% (kHz) |
|---|---|---|---|
| Improved Howland current source | 30 | 160 | 330 |
| Dual op-amp Howland current source | 20 | 130 | 250 |

on Fig. 4 and Eq. 12, the output impedance reduction reduces the output current delivered to the load and as a result, the relative error increases. Figure 9 also illustrates that dual op-amp Howland current source has less relative error compared to the improved Howland current source. As shown in the previous section, at low frequencies, increasing the tolerance of the resistors decreases the output impedance of the current source, and this reduction increases the relative error of both structures, and thus their errors are deviating from the ideal state. However, according to the results presented in the previous section, the tolerance of the resistors does not affect the current source output impedance at high frequencies, and its impact can thus be ignored. As a consequence, by increasing the frequency, the relative errors for various tolerance values approach and finally match the ideal state.

According to Fig. 9, the matching frequency of relative error to the ideal state directly related to the tolerance value of the circuit resistors. Thus, in the EIST system, to gain wider bandwidth and less relative error in the current amplitude, it is required to employ resistors with smaller tolerances. Table 1 presents the minimum operating frequencies as tolerance neutralization frequency at which the values of relative error match error in an ideal state for three tolerances. In fact, in these operating frequencies, the undesired impact of resistors tolerance is canceled. Using Table 1, it can be inferred that for equal tolerance, the minimum operating frequency of dual op-amp Howland current source is less than Howland current source. This means that for an identical tolerance value, the dual op-amp Howland gives wider bandwidth for EIST application.

## 6 Conclusion

In this paper, two different structures of the Howland current source for using in an EIST system were studied. It was shown that the tolerance of circuit resistors could affect both output impedance and output current amplitude. The simulation results show that the output impedance of the current sources is inversely proportional to tolerance. In low frequencies, the tolerance of the resistors results in a significant reduction in output impedance. In addition, it was shown that the use of lower tolerance resistors improves the frequency response of current sources. Therefore, by using more accurate resistors, wider bandwidth can be employed in spectral impedance tomographic systems. Based on the simulations and also according to the studied structures, it can be concluded that dual op-amp Howland current source

demonstrates lower impedance loss in the presence of tolerance, compared to the improved Howland current source.

Moreover, the relative error analysis of the improved Howland and dual op-amp Howland current source revealed that the operating frequency at which the impact of resistors' tolerance neutralized are different, affecting the bandwidth of the current source. For instance, for the resistors with 1% tolerance, the tolerance neutralization frequency was 250 kHz for dual op-amp Howland current source while in the other configuration the frequency was equal to 330 kHz. By decreasing the tolerance of the resistors, the difference between these frequencies reduced. However, the neutralization frequency of the dual op-amp Howland current source is always lower than the improved Howland current source and thus the dual op-amp Howland current source has better performance and more appropriate choice for an EIST system.

**Acknowledgements** Authors would like to express their sincere thanks to anonymous reviewers for their appreciative and constructive comments on the draft of this paper.

### Compliance with Ethical Standards

**Conflict of interest** The authors declare that they have no conflict of interest.

## References

1. Henderson, R. P., & Webster, J. G. (1978). An impedance camera for spatially specific measurements of the thorax. *IEEE Transactions on Biomedical Engineering, 3,* 250–254.
2. Nahvi, M., & Hoyle, B. (2008). Wideband electrical impedance tomography. *Measurement Science & Technology, 19*(9), 094011.
3. Silvera-Tawil, D., Rye, D., Soleimani, M., & Velonaki, M. (2015). Electrical impedance tomography for artificial sensitive robotic skin: A review. *IEEE Sensors Journal, 15*(4), 2001–2016.
4. Nahvi, M., & Hoyle, B. S. (2009). Electrical impedance spectroscopy sensing for industrial processes. *IEEE Sensors Journal, 9*(12), 1808–1816.
5. Baidillah, M. R., Iman, A.-A. S., Sun, Y., & Takei, M. (2017). Electrical impedance spectro-tomography based on dielectric relaxation model. *IEEE Sensors Journal, 17*(24), 8251–8262.
6. Nahvi, M., & Hoyle, B. S. (2009). Data fusion for electrical spectro-tomography. *IEEE international workshop on imaging systems and techniques (IST 2009)* (pp. 229–234).
7. Veal, B., Baldo, P., Paulikas, A., & Eastman, J. (2015). Understanding artifacts in impedance spectroscopy. *Journal of the Electrochemical Society, 162*(1), 47–57.
8. Dimas, C., Tsampas, P., Ouzounoglou, N., & Sotiriadis, P. P. (2017). Development of a modular 64-electrodes electrical impedance tomography system. In *Proceedings of 6th international conference on modern circuits and systems technologies (MOCAST 2017)* (pp. 1–4).
9. Nahvi, M., Hoyle, B. S., & Zhao, Y. (2010). Experimental verification trials for fast spectro-tomography sensing in process reactors. In *Proceedings of 6th World Congress on Industrial Process Tomography (ISIPT 2010).*
10. Brown, B., & Seagar, A. (1987). The Sheffield data collection system. *Clinical Physics and Physiological Measurement, 8*(4A), 91.
11. Rivera, D., Gaikwad, S., & Chen, X. (1994). CONTROL-ID: A demonstration prototype for control-relevant identification. In *Proceedings of IEEE American Control Conference* (pp. 2055–2059).
12. Nahvi, M., & Hoyle, B. S. (2009). Wideband excitation signals for electrical impedance industrial process tomography. In *Proceedings of the 5th international symposium on process tomography, Zakopane, Poland.*
13. Sanchez, B., Vandersteen, G., Bragos, R., & Schoukens, J. (2012). Basics of broadband impedance spectroscopy measurements using periodic excitations. *Measurement Science & Technology, 23*(10), 105501.

14. Nahvi, M. (2008). *Wideband electrical impedance spectro-tomographic imaging*. University of Leeds, Leeds, UK.
15. Islam, S. M. M., Reza, M. A. R., & Kiber, M. A. (2013). Development of multi-frequency electrical impedance spectroscopy (EIS) system for early detection of breast cancer. *International Journal of Electronics Informations, 2*(1), 26–32.
16. Heidari, A., Zanganeh, M., Nahvi, M. & Nihtianov, S. (2013). The impact of resistor mismatches and Op-amp limited GBW on the output impedance of the howland current source for EIT applications. In *Proceedings of 13th international scientific conference electronics (ET2013)* .
17. Hayt, W. H., Kemmerly, J. E., & Durbin, S. M. (1986). *Engineering circuit analysis*. New York: McGraw-Hill.
18. Chua, L. O., Desoer, C. A., & Kuh, E. S. (1987). *Linear and nonlinear circuits*. New York: McGraw-Hill College.
19. Armstrong, S., & Jennings, D. (2004). Current injection electrodes for electrical impedance tomography. *Physiological Measurement, 25*(4), 797.
20. Dickin, F., & Wang, M. (1995). Impedance sensors-conducting system. *Process Tomography-Principles, Techniques and Application*, 63–84.
21. Denyer, C., Lidgey, F., Zhu, Q., & McLeod, C (1993). High output impedance voltage controlled current source for bio-impedance instrumentation. In *Proceedings of 15th IEEE annual international conference of the engineering in medicine and biology society* (pp. 1026–1027).
22. Denyer, C., Lidgey, F., Zhu, Q., & McLeod, C. (1994). A high output impedance current source. *Physiological Measurement, 15*(2A), A79.
23. Saulnier, G. J., Cook, R., Gisser, D., Goble, J., Hochgraf, C., Isaacson, D., et al. (1991). A high-speed, high-precision electrical impedance tomograph. In *Proceedings of the annual international conference of the IEEE engineering in medicine and biology society* (vol. 13, pp. 5–6).
24. Sheingold, D. (1964). Impedance & admittance transformations using operational amplifiers. *Lightning Empiricist, 12*(1), 1–8.
25. Ross, A. S., Saulnier, G., Newell, J., & Isaacson, D. (2003). Current source design for electrical impedance tomography. *Physiological Measurement, 24*(2), 509.
26. Wilson, A., Milnes, P., Waterworth, A., Smallwood, R., & Brown, B. (2001). Mk3. 5: a modular, multi-frequency successor to the Mk3a EIS/EIT system. *Physiological Measurement, 22*(1), 49.
27. Russo, S., Nefti-Meziani, S., Carbonaro, N., & Tognetti, A. (2017). Development of a high-speed current injection and voltage measurement system for electrical impedance tomography-based stretchable sensors. *Technologies, 5*(3), 48.
28. Yerworth, R. J., Bayford, R., Brown, B., Milnes, P., Conway, M., & Holder, D. S. (2003). Electrical impedance tomography spectroscopy (EITS) for human head imaging. *Physiological Measurement, 24*(2), 477.
29. AnalogDevices. 60 MHz 2000 V/μs Monolithic Operational Amplifier AD844. *datasheet*.
30. Casas, O., Rosell, J., Bragós, R., Lozano, A., & Riu, P. (1996). A parallel broadband real-time system for electrical impedance tomography. *Physiological Measurement, 17*(4A), A1.
31. Wang, M., Ma, Y., Holliday, N., Dai, Y., Williams, R. A., & Lucas, G. (2005). A high-performance EIT system. *IEEE Sensors Journal, 5*(2), 289–299.
32. Bragos, R., Rosell, J., & Riu, P. (1994). A wide-band AC-coupled current source for electrical impedance tomography. *Physiological Measurement, 15*(2A), A91.
33. Pease, R. A. (2008). A comprehensive study of the Howland current pump. *National Semiconductor. January, 29*.
34. Wang, W., Brien, M., Gu, D., & Yang, J. A.. (2007). A comprehensive study on current source circuits. In *Proceedings of 13th international conference on electrical bioimpedance and the 8th conference on electrical impedance tomography* (pp. 213–216).
35. Holder, D. S. (2004). *Electrical impedance tomography: methods, history and applications*. Cambridge: CRC Press.
36. Bouchaala, D., Kanoun, O., & Derbel, N. (2016). High accurate and wideband current excitation for bioimpedance health monitoring systems. *Measurement, 79,* 339–348.
37. Franco, S. (2015). *Design with operational amplifiers and analog integrated circuits*. New York: McGraw-Hill.
38. Cole, K. S. (1928). Electric impedance of suspensions of spheres. *The Journal of General Physiology, 12*(1), 29–36.

39. Kusche, R., Malhotra, A., Ryschka, M., Ardelt, G., Klimach, P., & Kaufmann, S. (2015). A FPGA-based broadband eit system for complex bioimpedance measurements—Design and performance estimation. *Electronics, 4*(3), 507–525.
40. Martinsen, O. G., & Grimnes, S. (2015). Bioimpedance and bioelectricity basics. (3rd ed.), Cambridge: Academic Press.